DIAGNOSTIC TOOLS FOR ULTRA-LOW EMITTANCE AND ULTRA-SHORT ELECTRON BUNCHES

H. Schlarb, DESY, Hamburg, Germany

Abstract

The operation of future linear colliders and X-ray Free Electron Lasers places stringent demands on the required beam quality. Setting up and optimization of the machine requires reliable and effective beam diagnostics tools. Different measurement methods and reconstruction techniques for both the transverse and longitudinal phase space distributions are discussed.

1 INTRODUCTION

In order to achieve the luminosity required for high energy experiments in a e^+e^- linear collider, the flat electron and positron beams leaving the damping rings and accelerated in the main linac have to be focused down to vertical spot size of a few nanometers at the interaction point (IP). Emittance dilution e.g. occur due to wakefields and dispersion along the linac, coherent or incoherent synchrotron radiation in the arcs of the beam line, as well as a betatron coupling between horizontal and vertical direction. To preserve the low emittance the transverse beam distribution is measured at various positions along the entire linac and the Beam Delivery System (BDS). Clearly the most challenging measurements are those at the IP. But also the profile monitors required at the BDS have to deal with spot sizes in the range of micrometer horizontally and a few hundred nanometers vertically.

Compared to that, the typical beam sizes with equal beam emittance in horizontal and vertical direction of a linac driven Free Electron Laser (FEL) are more relaxed. But the requirement on the peak current to drive the laser beam into saturation is stronger, in the order of several kA. For that, a high brilliance electron beam produced at an rf gun based photo injector is compressed in several steps to bunch length of approximately 20 μm combining off-crest acceleration with magnetic chicane. Preserving the required transverse emittance of 1 μm and simultaneously the longitudinal emittance of 25 eV m at this bunch length will be the most challenging task for the FEL operation. Precise measurements of the longitudinal beam profile behind the bunch compressor stages is a stringent demand for a successful operation of X-ray FELs.

2 TRANSVERSE BEAM DISTRIBUTION AND EMITTANCE MEASUREMENTS

The particle distribution in phase space (x, x') and (y, y') is usually described by an ellipse. The ellipse is characterized by three independent parameters, for instance the three second-order moments $<x^2>$, $<x'^2>$, and $<xx'>$, or equivalently, by the emittance and the Twiss-parameters $(\epsilon, \beta, \alpha)$. At energies of a few 10 MeV a multi-slit mask can be used to measure all moments within a single electron pulse [1]. At higher energy the beam angular divergence $<x'^2>$ and correlation $<xx'>$ are difficult to measure, while various techniques have been developed to measure the transverse beam distribution. To determine the beam emittance in this case, either the transfer function of the beam to the profile monitor can be varied using a set of quadrupoles (quadrupole scans) or the beam profiles have to be measured at several points along the beam line separated by a sufficient betatron phase advance.

2.1 Beam profile monitors

Optical transition radiation One important method to monitor the beam profile is the use of optical transition radiation. Thin mirror finished metal foils are commonly used as radiators.

When a charged particle crosses the interface of two media with different dielectric constants transition radiation (TR) is emitted both in the backward and forward direction. Up to the plasma frequency of the metal foil the radiation intensity does not depend on frequency (for a foil of infinite extension). For wavelengths λ much smaller than the bunch length σ_z the individual contributions of TR from the particles in a bunch add up incoherently. The wavelength range between 400 nm and 800 nm (optic transition radiation OTR) can be used for transverse beam profile measurements. The angular intensity distribution of TR for a single particle can be described in far field region by the Ginzburg-Frank formula [2]. For ultra-relativistic energies ($\gamma \gg 1$) the angular distribution is approximately given by [3]

$$\frac{d^2W}{d\omega d\Omega} \propto \left(\frac{\theta}{\gamma^{-2}+\theta^2}\right)^2, \quad \theta \ll 1, \tag{1}$$

where θ is the angle with respect to the electron velocity (forward OTR) or to the direction of the specular reflection (backward OTR). The emission of photons are peaked at an angle $1/\gamma$ but the intensity falloff outside the $1/\gamma$ cone is slow and the tails are independent on the particle energy. The spatial resolution d, is limited by diffraction. The relevant parameter is the collection angle θ_0 of the optical system. The size of single electron OTR diffraction pattern calculated in vector wave theory is [4]:

$$d_{FWHM} \approx 1.44\frac{\lambda}{\theta_0}, \quad \gamma\theta_0 \gg 1. \tag{2}$$

This value for the radially polarized OTR is about 3 times larger than for the unpolarized radiation from a point source. Further details on the resolution, the effect of polarizer and mask, the requirements on the camera system

and the reconstruction of the image can be found in [4, 5] With a typical collecting angle of 0.1 rad and a wavelength of 500 nm the expected resolution is about 5-10 μm. So far, the smallest measured beam size with OTR is about 50 μm at an electron beam energy of 30 GeV [6].

Synchrotron Radiation (SR) The most fundamental diagnostic in an storage ring is the beam profile measurement via imaging of the visible SR. The resolution of this monitor is limited by diffraction to beam sizes of about 20 μm [7]. By measuring the spatial coherency of the SR beam using a double slit configuration (SR interferometer) the resolution can be significantly improved [8]. Alternatively, the diffraction effects is reduced for X-ray imaging of the electron beam through a pinhole system [9]. Both methods can resolve beam sizes in the micrometer regime and are applicable for the BDS.

Wire scanner Wire scanners are commonly in use at storage rings [10] and linacs [11]. A thin wire is moved transversely across the path of the beam. The electrons intercepting the wire are scattered and generate bremsstrahlung photons which both can be detected downstream the scanner. Thus, a scan across the beam yields the intensity profile.
The resolution is limited by the smallest practical wire diameter and the accuracy of the wire translation. Carbon fibers down to 4 μm diameter [12, 13] have been used, resulting in a rms-resolution of about 1 μm. Positioning accuracy in the sub-micron regime is achieved using precise stepping motors in combination with optical encoders. The beam position and beam current are monitored to correct for jitter and charge fluctuations. Breakage of carbon wires caused by thermal heating and thermal stress has been observed for charge densities exceeding 0.5 nC/μm^2 accumulated within a pulse train [14]. For micron beam sizes this limit is reached in a single shot for a bunch of a few nC.

Laser wire scanner Instead of a solid wire, a high intense laser beam being an indestructible target can be applied to measure the transverse beam profile. Compton scattered photons or electrons are detected. This technique has been successfully applied at SLC for a beam size down to 1 μm [15]. Here, the electron beam was moved across the laser beam.
In order to achieve a sufficiently small waist, the laser beam is focused to its diffraction limit given by (with a gaussian profile)

$$\sigma_L = \frac{\lambda}{2\pi\theta} \tag{3}$$

where λ is the wavelength and θ the opening angle of the laser beam as sketched in Fig. 1. The distance over which the laser beam diverges to $\sqrt{2}$ of its minimum size $2 \cdot x_R = 8\pi\sigma_L^2/\lambda$ (Rayleigh range) defines the usable length of the laser wire. Typically lasers can be focused down to about $\sigma \approx 1.2\,\sigma_L$. For an opening angle θ of 10° the resolution using a fourth harmonic Nd:YLF laser ($\lambda = 262$ nm) yields

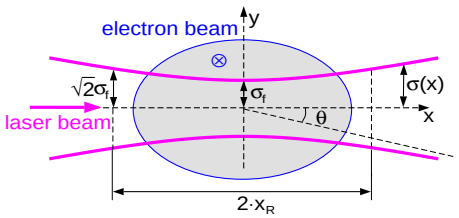

Figure 1: Scheme of a gaussian laser beam focused to its diffraction limit.

$\sigma_L \approx 300$ nm with $2 \cdot x_R \approx 6\,\mu$m.
The Compton cross section is in the order of 0.1 to 0.6 barn depending on the electron beam energy and the wavelength of the laser (see e.g. [16]). Even for spot sizes of 1 μm the peak power of the laser must be in the order of MW to yield a few thousand Compton photons per bunch [17].

Laser interferometer Towards beam sizes in the nanometer range, a standing wave interference pattern generated by crossing two laser beams has been proposed by [18] and successfully tested at the FFTB experiment [19]. The fringe spacing d of the interference pattern depends on

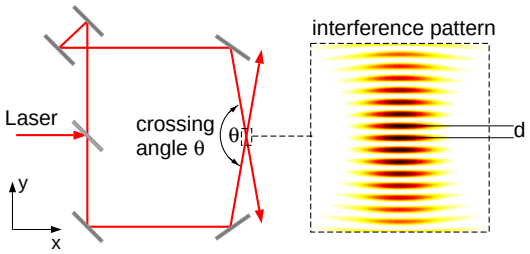

Figure 2: Schema of the generation of an interference pattern using a split laser beam. d is the fringe spacing.

the laser wavelength λ and the crossing angle:

$$d = \frac{\lambda}{2 \cdot \sin(\theta/2)}. \tag{4}$$

The electron beam is moved over the pattern and a modulation M of the counting rate of the Compton scattered photons is observed,

$$M = \frac{N_+ - N_-}{N_+ + N_-} = |\cos(\theta)| \exp\left[-2\left(\frac{\pi\sigma_y}{d}\right)^2\right]. \tag{5}$$

The modulation M vanishes if the vertical beam size σ_y is large compared to the fringe spacing ($\sigma_y \gg d$), while for a infinite small beam ($\sigma_y \ll d$) M is equal to the maximum modulation of the laser interference pattern, as sketched in Fig. 3. At the FFTB a Nd:YAG laser ($\lambda = 1064$ nm) was used to measure vertical rms-beam size between 40 nm and 720 nm with crossing angles of 174° and 30°. The smallest observed beam spot was about 58 nm [16]. A crossing angle of 6° was used to measure the horizontal rms-beam sizes in the range between 0.76 μm and 3.4 μm [20].

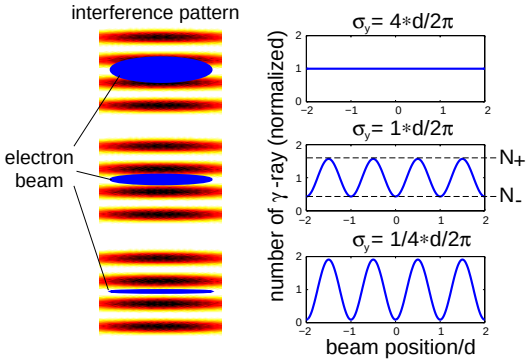

Figure 3: Modulation of Compton scattered photons as a function of the vertical electron beam position for different beam sizes (top large, center medium, bottom small)

This demonstrates the flexibility of the laser interferometer if different crossing angles can be realized.
The measurement ranges given above assume that modulations M from 10% to 90% can be resolved. The resolution of the interferometer with a forth harmonic laser Nd:YAG ($\lambda = 266$ nm) for $M = 90\%$ is estimated to be 10 nm. The potential difficulties will be the spatial and temporal coherence of the laser beam in the ultra violet, as well as to cope with beam jitter and mechanical vibrations. The effort to build such a system will be considerable. A discussion on systematic errors for the laser interferometer technique is found in [16].

2.2 *Emittance analysis and reconstruction techniques*

The standard technique to extract the beam emittance and the Twiss-parameters from beam profile measurements is the parabola fit analysis. The second order moments at a given point in the beam line are transformed according to [21]

$$\frac{<x^2>_i}{S_i^2} = \left(\frac{C_i}{S_i}\right)^2 <x^2>_0 - 2\left(\frac{C_i}{S_i}\right) <xx'>_0 + <x'^2>_0 \tag{6}$$

where S and C are the sine and cosine like functions of the beam transfer matrix. The index i indicates the individual measurements. By fitting the parameters $<x^2>_0, <x'^2>_0$, and $<xx'>_0$ in Eq.6 which depend quadratically on the ratio (C/S) one gets the best ellipse approximating the 2-dimensional phase space distribution. In case of non-gaussian tails e.g. due to transverse wake fields, the ellipse does not describe the core of the beam correctly. In that case, a reconstruction of the complete initial phase space is helpful, e.g. using the transverse phase space tomography.

The measured beam projection $\rho(x)$ is related to a projection of the initial phase space distribution $\rho_0(x_0, x_0')$ to a coordinate system (u, v) which is rotated by an angle ϕ determined by

$$\cos(\phi) = \frac{C}{N}, \quad N = \sqrt{C^2 + S^2}. \tag{7}$$

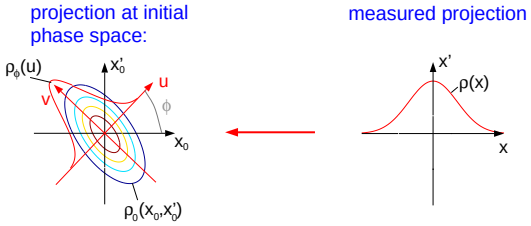

Figure 4: The horizontal beam profile at a downstream beam profile monitor (right hand side) can be related to the projection of the initial phase space distribution onto an axis u of a rotated coordinate system (u, v) (left hand side).

This is illustrated in Fig. 4. The projection $\rho_\phi(u)$ is also called the Radon transform of $\rho_0(x_0, x_0')$:

$$\rho_\phi(u) = \int_{u=\cos(\phi)x_0+\sin(\phi)x_0'} dv\, \rho_0(x_0, x_0') = N \cdot \rho(x), \quad u = \frac{x}{N}. \tag{8}$$

The factor N takes into account the shearing of the transverse phase space, while transporting the beam through a magnetic lattice. By varying the rotation angle ϕ in small steps over an interval π, the initial particle distribution can be reconstructed applying the inverse Radon transformation [22]. Fig. 5 shows a reconstructed vertical phase space measured at the injector of the TESLA Test Facility. The diagnostic power of this technique revealed a second beam spot caused by a spurious reflection at the laser system for the photo cathode rf gun.

A filtered back-projection algorithm was used as basis for the numerical treatment of the data. A discussion of the reconstruction artifacts and the incorporation of space charge effects is given in [23].

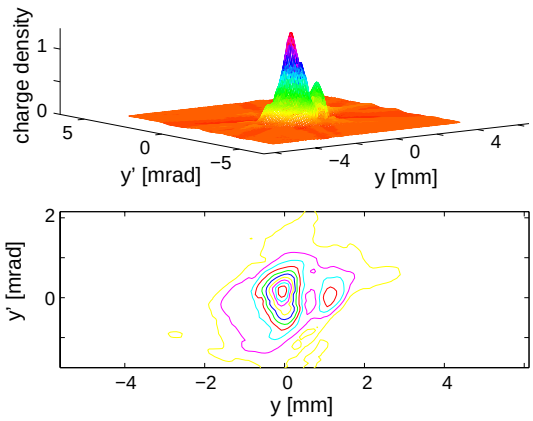

Figure 5: Reconstruction of the vertical phase space distribution from a quadrupole scan performed at the TTF-injector. Upper graph: three dimensional view. Lower graph: contour plot.

3 LONGITUDINAL CHARGE DISTRIBUTION AND BUNCH LENGTH MEASUREMENTS

3.1 *Frequency domain measurements*

Coherent Transition Radiation (CTR) can be used to determine the longitudinal charge distribution. The spectral intensity emitted by a bunch of N particles is

$$I_{tot} = I_s(\omega)\left(N + N(N-1)|f(\omega)|^2\right) \qquad (9)$$

where $I_s(\omega)$ is the intensity radiated by a single electron at a given frequency ω and $f(\omega)$ the longitudinal form factor of the bunch [24]. For wavelengths in the order of the bunch length the form factor approaches unity. The intensity of the coherent part of the radiation spectrum is enhanced by the square of the number of particles. The enhancement permits a direct measurement of $|f(\omega)|^2$.

Martin-Puplett interferometer Commonly used is a Martin-Puplett interferometer (Fig. 6) to measure the autocorrelation of an electron bunch [25]. Wire grids are used to polarize and split the radiation into two beams. The polarization is flipped by the roof mirrors and the initially reflecting beam splitter is now transmitting and vice versa. The recombined radiation is elliptically polarized, depending on the path difference between the two arms. The vertical and horizontal component of the polarization is measured by two broad band detectors.

A Fourier transformation of the autocorrelation function

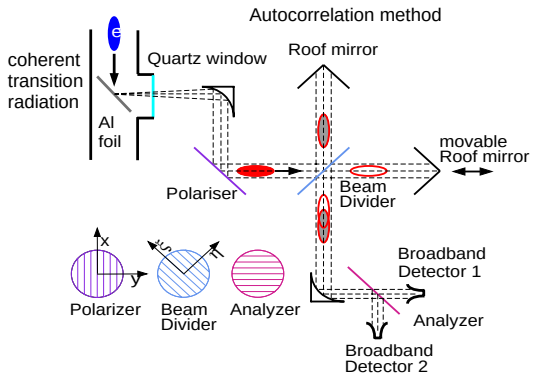

Figure 6: Martin-Puplett Interferometer

yields the magnitude $|f(\omega)|$ of the from factor. By means of the Kramers-Kronig relation to compute the phase of the form factor, the longitudinal charge distribution can be calculated.

Frequency dependent correction due to the finite screen size and aperture, the transmission through the quartz window, the reflectivity of the wire grids and the response function of the detector requires an extrapolation to low frequencies and systematic corrections to high frequencies.

This technique can be applied in the frequency range between 50 GHz to 3 THz. Above 3 THz, wire grids can not be winded anymore, but a Mylar foil can be used as beam splitter in a standard Michelson interferometer setup. At the Stanford SUNSHINE facility, electron pulses with rms-bunch lengths below 20 μm have been measured [26].

3.2 *Time domain measurements*

Streak camera A streak camera is a device for a direct (single-shot) determination of the longitudinal bunch charge distribution. A light pulse generated by the electron bunch by synchrotron, Cherenkov, or optical transition radiation travels through a dispersion-free optical system, a wavelength filter and a slit before hitting the photo-cathode of the streak camera. The slit width of the streak camera should be set under the trade-off between the requirement of the a time-resolution and the signal to noise ratio.

The present resolution limit of commercial available streak camera is 200 fs (FWHM). The shortest bunch length measured with a state-of-the-art streak camera at the University of Tokyo using a BNL-type rf photo-injector in combination with a magnetic bunch compressor was 440 femtoseconds (FWHM) [27].

Electro-optic sampling The method is based on the detection of the co-traveling electric field of a relativistic electron bunch when it passes close to a non-linear optical crystal. The electric field induces birefringence which is probed by a synchronized femtosecond Ti:Sapphire laser pulse. The initial linearly polarized laser pulse becomes elliptically polarized, whose ellipticity is measured using a combination of a quarter wave plate, a Wollaston prism and a balanced detector. This new technique has been tested at the FELIX FEL in the Netherlands [28]. The longitudinal

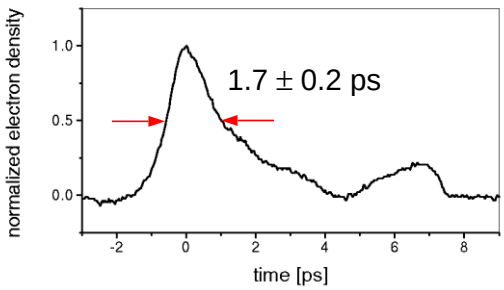

Figure 7: Measurement of the longitudinal bunch profile at FELIX using electro-optic sampling.

electron bunch profile has been measured at the entrance of the undulator inside the vacuum chamber. A 0.5 mm thick ZnTe crystal (<110> oriented) has been used as an electro-optic sensor. The crystal was placed in a distance of 6 mm perpendicular to the propagation of the electron beam. A 12 fs Ti:Sapphire laser was synchronized to the accelerator rf. The electron pulse train has been swept via an rf-phase shifter over the laser pulse train, such that a complete electric profile is measured within a few microseconds. Due to this rapid scanning technique the jitter between electron

and laser pulse train was negligible small, only 50 fs [29]. Electron pulses down to 1.7 ps (FWHM) have been measured (Fig. 7) with a resolution of better than 800 fs. The achievable time resolution of about 100 to 200 fs is limited by the excitation of phonon resonances in the nonlinear crystal which distort and attenuate the electric field pulse.
The method can be extended to a single-shot measurement [30]. For that, the ultra-short laser pulse of a pulse length t_i is chirped (long wavelengths are leading the short wavelengths) to a length t_s of some picoseconds. The temporal distribution of the electron bunch is obtained using a diffraction grating and a CCD camera. The time resolution is then reduced to $t = \sqrt{t_s \cdot t_i}$.

Off-phase rf-acceleration A time slice in an electron bunch accelerated at an off-crest phase receives an energy increment that varies with the arrival time. The correlation between the temporal distribution of the bunch and the energy distribution can be observed at an profile monitor behind an energy spectrometer. The energy distribution is measured at different acceleration phases. This allows to eliminate the initial energy spread of the beam and to determine the longitudinal charge density [31]. Moreover, applying a special reconstruction technique similar to that described in section 2.2, the full longitudinal phase space distribution can be obtained [32].
The use of a longitudinal dispersive magnetic chicane before the off-phase acceleration can eliminate the effect of initial energy spread from the final measurement [33, 23]. The technique is limited by the resolution of the spectrometer, the achievable beta function at the profile monitor in the spectrometer arm, and the validity of linear beam transfer. For short bunch length and high bunch charge nonlinear effects due to space charge, wakefields, or coherent synchrotron radiation have to be take into account. At Stanford Picosecond FEL Center the method was used to observe the modulated profile of a microbunched electron beam at the exit of a far-infrared FEL-oscillator [34]. A time resolution of approximately 100 fs has been reached.

4 CONCLUSIONS

Several techniques have been presented to meet the challenges of transverse and longitudinal beam profile measurements for future linear colliders and X-ray FELs.

5 ACKNOWLEDGMENTS

The author would like to thank S. Schreiber, K. Honkavaara, P. Schmuser and A. Swiderski for valuable discussions.

6 REFERENCES

[1] H. Edwards et al., Proc. 21^{st} Int. FEL Conf., Hamburg (1999).

[2] V.L. Ginzburg et al., Sov. Phys. JETP 16, 15 (1946).

[3] L. Wartski et al., J. Appl. Phys. 46, 3644 (1975).

[4] V.A. Lebedev, Nucl. Inst. A372, 344 (1996).

[5] D.W. Rule and R.B. Fiorito, Proc. 1993 Part. Accel. Conf., Washington DC, May 1993, p. 2453; J.-C. Denard et al., Proc 1997 Part. Accel. Conf., Vancover; X. Artru et al., Nucl. Inst. A 410, 148 (1998); M. Castellano and V.A. Verzilov, Phys. Rev. ST Accel. Beams 1, 062801 (1998); K. Honkavaara et al., Particle Accelerators, Vol 63, 147 (1999).

[6] P. Catravas et al., Proc. 1999 Part. Accel. Conf., New York.

[7] A. Hofmann et al., Nucl. Inst. and Methods A 203, 483 (1992); M. Ferianis, Proc. 1998 Euro. Part. Accel. Conf, Stockholm; N. V. Smolyakov et al., Proc. 1998 Euro. Part. Accel. Conf, Stockholm.

[8] T. Mitsuhashi et al, Proc. 1998 Euro. Part. Accel. Conf, Stockholm; S. Hiramatsu et al., Proc 1999 Part. Accel. Conf., New York; H. Hayano et al., Proc 1999 Part. Accel. Conf., New York.

[9] P. Elleaume et al.,J. Synch. Radiation 2,209 (1995); Z. Cai et al., Rev. Sci. Instrum. 67 (9) Sept. (1996).

[10] B. Bouchet et al., Proc. 1991 IEEE Part. Accel. Conf., San-Francisco (1991).

[11] M. Ross, Proc. Workshop Accel. Inst. 2, ed. ES McCrory. New York: AIP (1995).

[12] C. Field, Nucl. Inst. and Methode A 360,467 (1995).

[13] D. McCormick et al., Proc. Beam. Inst. Workshop 6, New York: AIP (1995).

[14] C. Field et al., Proc. Beam Inst. Wkshp. 8, New York:AIP Press p. 440 (1998).

[15] M. Ross et al., Proc. Beam Inst. Wkshp. 7,New York (1997).

[16] P. Tenenbaum and T. Shintake, Annu. Rev. Nucl. Part. Sci. 49, p. 125 (1999).

[17] R. Alley et al., Nucl. Inst. and Methods A 379,363 (1996).

[18] T. Shintake, Nucl. Instr. and Methods A 311,453 (1992).

[19] V. Balakin et al., Phys. Rev. Let. Vol. 74, 13, p. 2478 (1995).

[20] T. Shintake, Beam Inst. Workshop, ANL, Argonne (1996)

[21] H. Wiedemann, Particle Accelerator Physics, Berlin: Springer-Verlag (1993).

[22] J. Radon, Ber. Verh. Saechs. Akad. Leipzig, Math. Phys. Kl. 69 (1917) 262.

[23] M. A. Geitz, DESY-THESIS-1999-033, (1999).

[24] J.S. Nodvick et al., Phys. Rev. A, Vol. 96, No. 2 (1954).

[25] M. Ding et al., Nucl. Instr. and Methods A 393,504 (1997); B. Leisser et al., Proc. 1999 Part. Accel. Conf., New York (1999); G. A. Krafft et al., Proc. of EPAC 98 (1998).

[26] P. Kung et al., SLAC-PUB-6507, (1994).

[27] M. Uesaka et al., Proc. of 8^{th} AAC Wkshp.,Baltimore (1998).

[28] D. Oepts et al., Proc. 21^{st} Int. FEL Conf., Hamburg (1999).

[29] G.M.H. Knippels et al., Phys. Rev. Lett. 83,1578 (1999).

[30] I. Wilke et al., DESY Report to be published (2000).

[31] D.X. Wang et al., Phys. Rev. E 57, 2, p. 2283 (1998)

[32] M. Huening et al., DESY Report to be published (2000)

[33] K.N. Ricci et al., Nucl. Inst. and Methods A 445,363 (2000).

[34] K.N. Ricci et al., Phys. Rev. ST Accel. Beams. 3, 032801 (1998).